AIAA JOURNAL
Vol. 45, No. 4, April 2007

Meshless Local Petrov–Galerkin Formulation for Problems in Composite Micromechanics

Thi D. Dang* and Bhavani V. Sankar†
University of Florida, Gainesville, Florida 32611- 6250

DOI: 10.2514/1.23434

In this paper we present the meshless local Petrov–Galerkin formulation for the generalized plane strain problem with specific emphasis on micromechanics of composite materials containing material discontinuities. The problem requires the introduction of an extra discrete degree of freedom, the out-of-plane uniform normal strain. The treatment of material discontinuity at the interface between the two phases of the composite is presented by means of direct imposition of interface boundary conditions. The meshless local Petrov–Galerkin method is used in the micromechanical model for predicting the elastic constants of the composite. To our knowledge, this is the first study in which the meshless local Petrov–Galerkin method is formulated for the so-called meshless local Petrov–Galerkin method based micromechanical analysis. Examples are presented to illustrate the effectiveness of the current method, and it is validated by comparing the results with available analytical and numerical solutions. The current method has the potential for use in micromechanics, especially for textile composites, where the meshing of the unit cell has been quite difficult.

Nomenclature

a	=	width, height, and depth of unit cell
$\mathbf{a}(\mathbf{x})$	=	vector of unknown parameters $a_j(\boldsymbol{x})$
b_i	=	body force
$\mathbf{C}$	=	constant matrix of homogeneous composite
c_i	=	distance from node i to its third nearest neighboring node
d_i	=	distance from the sampling point $\mathbf{x}$ to the node $\mathbf{x}_i$
E	=	Young's modulus
$\mathbf{I}$	=	identity matrix
$\mathbf{J}(\mathbf{x})$	=	weighted discrete L_2 norm
k	=	parameter in the Gaussian weight function ($k = 1$)
L_s	=	part of local boundary over which no boundary conditions are specified
N	=	total number of nodes
n	=	number of points in the neighborhood of $\mathbf{x}$ for which $w(\mathbf{x} - \mathbf{x}_i) > 0$
n_i	=	unit outward normal to the boundary
$\mathbf{P}^T(\mathbf{x})$	=	vector of the complete monomial basis of order $m(m = 3)$
r_i	=	radius of the domain of influence of the weight function ($r_i = 4c_i$)
r_0	=	radius of the local domain
r_s	=	part of the local boundary located on the global boundary
$\bar{t}_i$	=	prescribed traction on the boundary Γ_t
u, v, w	=	u_1, u_2, u_3
$\hat{u}_b$	=	fictitious displacement on the interface
u_i	=	displacement field (trial function)
$\hat{u}_i$	=	fictitious nodal value
$\bar{u}_i$	=	prescribed displacement on the boundary Γ_u
$\tilde{u}_i$	=	actual displacement on the interface
$u^h(\mathbf{x})$	=	moving least-squares approximation
V	=	volume of unit cell
V_f	=	fiber volume fraction
v_i	=	test function
$w(\boldsymbol{x} - \mathbf{x}_i)$	=	weight function
x_1, x_2, x_3	=	Cartesian coordinates
α	=	penalty parameter ($\alpha = 10^8$)
δ_{ij}	=	Kronecker delta
$\boldsymbol{\varepsilon}_v$	=	strain matrix computed from the test function
ε^0	=	constant macroscopic direct strain in the z direction
$\boldsymbol{\varepsilon}^M$	=	macroscopic level strain matrix
ν	=	Poisson's ratio
σ_{ij}	=	Cauchy stress tensor
$\boldsymbol{\sigma}^M$	=	macroscopic level strain matrix
$\phi(\mathbf{x})$	=	shape function
ϕ_b, ϕ_r	=	subsets of ϕ w.r.t. nodes on the interface and within the material
Ω	=	global domain
Ω_s	=	local domain
$\partial\Omega$	=	boundary of the local domain Ω_s

I. Introduction

THE generalized plane strain formulation is widely used in many important problems, especially in the micromechanical analysis of composite materials to predict their stiffness and strength properties [1–4]. The presentation of the problem in the form of variational principles of the finite element method (FEM) has been documented systematically by Pagano and Soni [5] and Li and Lim [6]. Li and Lim [6] formulated the variational principles of the finite element method for the generalized plane strain problem by the introduction of an extra discrete degree of freedom in the third direction representing the out-of-plane direct strain. Although previously existing analyses are based on the FE methods, the analysis presented in this paper is based on the meshless local Petrov–Galerkin (MLPG) method by allowing an extra degree of freedom in the longitudinal direction representing the out-of-plane direct strain.

The finite element method has been successfully applied to many problems in mechanics of composite materials. It is a robust and thoroughly developed technique, but it is not without shortcomings. The reliance of the method on a mesh leads to complications for

Presented as Paper 1691 at the 47th AIAA/ASME/ASCE/AHS/ASC Structures, Structural Dynamics, and Materials Conference, Newport, RI, 1–4 May 2006; received 23 February 2006; revision received 28 September 2006; accepted for publication 16 October 2006.

*Graduate Student, Department of Mechanical and Aerospace Engineering. Student Member AIAA.

†Newton C. Ebaugh Professor, Department of Mechanical and Aerospace Engineering; sankar@ufl.edu. Associate Fellow AIAA (Corresponding Author).

certain classes of problems. For example, in the development of advanced composite materials, especially textile composites, one of the major technical barriers in modeling textile composites such as braided and woven composites is the finite element mesh generation. Actually, for composite materials with complex yarn architectures, the meshing of individual yarns in the unit cell is quite simple. However, the meshing of the interfacial region between matrix phases and individual yarns is much more difficult as shown by Kim and Swan [7]. The region is multiply connected, mesh in different phases may not be compatible, and it is difficult to get a suitable mesh on which opposite faces of the unit cell have identical nodes so that periodic boundary conditions can be implemented using multipoint constraints. The available finite element based methods are satisfactory for stiffness prediction because stiffness properties are based on volume averaging of stresses and strains in the representative volume element (RVE) of the composite, and the approximation involved in the FE meshing does not affect the results significantly. However, modeling the damage, especially progressive damage, requires an accurate description of the stress field in different phases and requires a very fine mesh [8,9]. The FEM based micromechanical models have been successfully employed in predicting thermoelastic constants of fiber reinforced composites materials; their use for strength prediction under multiaxial loading conditions is not practical as reported by Sankar et al. [9–11].

We expect that the tediousness and inaccuracies involved in mesh generation and hence inaccuracies in the results can be avoided using the new meshless techniques such as the MLPG method. The MLPG approach proposed by Atluri [12,13] is one of several meshless schemes. The main advantage of this method compared to other meshless methods is that no background mesh is used to evaluate the various integrals appearing in the local weak formulation of the problem. Therefore, this method is a truly meshless approach in terms of both interpolation of variables and integration of energy. The meshless methods have been demonstrated to be efficient in solving different problems [14–17]. In this paper the MLPG method is applied to micromechanics of composites. One of the major drawbacks in applying meshless methods to inhomogeneous material systems is the treatment of material discontinuity occuring at the fiber-matrix interface. The high-order continuity of the moving least-squares approximations (MLS), which is at least C^1, allows for continuity of displacements and stresses throughout the subdomain. However, the high-order continuity imposes a difficulty when considering the discontinuities of the derivatives at the interface of the inhomogeneous bodies, because the shape functions from the MLS approximations do not have the delta function properties. For the analysis of linear elastostatic problems by meshless methods, say the element free Galerkin method (EFG), Cordes and Moran [18] used the method of Lagrange multipliers; Krongauz and Belytschko [19] employed a special jump function at the line or the surface of discontinuity with parameters governing the strength of the discontinuity; and Cai and Zhu [20] used the direct imposition of essential boundary and interface conditions. Whereas Cordes and Moran studied a two-dimensional elastostatic problem, Krongauz and Belytschko as well as Cai and Zhu analyzed a one-dimensional elastostatic problem, all based on the EFG method. Recently Batra et al. [21] also used the MLPG method to analyze heat conduction in which the continuity of the normal component of the heat flux at the interface between two materials is satisfied either by the method of Langrange multipliers or by using a jump function.

Based on the previous work of Atluri [12,13], we propose a technique for the treatment of material discontinuity at the interface between the two phases of the composite by the MLPG method in which we use a penalty formulation to enforce the essential boundary conditions and find the actual displacements at the nodes on the material interface to impose the displacements directly. Also, in the current paper, the MLPG method based micromechanical model of a unidirectional fiber composite is performed by analyzing the unit cell or representative volume element of the composite. In this paper, an extra discrete degree of freedom representing the out-of-plane direct strain is included. More general forms, which include more discrete and/or continuum degrees of freedom following the same procedures are developed by Dang and Sankar [22]. Furthermore, only orthotropic materials with one of the material principal axes perpendicular to the plane under consideration are considered in this paper.

One of the major factors influencing the success of a methodology is the cost vs accuracy tradeoff. Comparison of computational cost between a meshless method and an FE solution with the same number of unknowns in low-order finite elements was carried out by Belytschko et al. [23], and Atluri [24]. It has been seen that the FE results are in general less expensive. However, comparing the costs based on a given level of accuracy or if high-order finite elements are compared, then the results can be quite different. The effort of researchers in improving the meshless methods in this aspect is still ongoing. The latest effort devoted to improving the effectiveness of the MLPG method can be found in Atluri and Shen [24,25] in which the authors introduce MLPG5 using the Heaviside function as the test function in each domain; thus the domain integral on each domain is altogether avoided in computing the stiffness matrix. It involves only boundary integrals over each circle (domain), which will greatly improve the effectiveness of the MLPG5 method and will make the solution stable, fast, and accurate. It is reported that the MLPG5 provides a simple and efficient alternative to the finite element and boundary element methods. The motivation of this paper is to provide a framework in which the MLPG formulation can be applied to micromechanical analysis of the composites. It is more general and thus it can be very useful in predicting the stiffness and strength properties of textile composites.

The paper is organized as follows. Section II gives a brief description of the MLS approximation, weak form, and discretization along with the generalized plane strain problem. The treatment of material discontinuity is also presented. Section III describes the MLPG-based micromechanical model for two-phase composites. The computation and discussion of results are given in Sec. IV. Conclusions are summarized in Sec. V.

II. Formulation of the Problem

A. MLS Approximation Scheme

In the following we provide a brief description of the MLS approximation and also the MLPG formulation for the sake of completion and also to introduce the various notations and definitions (see [24] for the details).

In the MLPG method, the shape functions $\phi_i(\mathbf{x})$ of the unknown trial function are found by the MLS approximation [26]. First, we consider a subdomain $\mathbf{\Omega}_\mathbf{x}$ called the domain of definition of the MLS approximation for the trial function at point x which is located in the problem domain $\mathbf{\Omega}$. The unknown trial approximation $u^h(\mathbf{x})$ of the function $u(\mathbf{x})$ is defined by

$$u^h(x) = \sum_{j=1}^{m} p_j(x) a_j(x) = \mathbf{p}^T(\mathbf{x})\mathbf{a}(\mathbf{x}) \tag{1}$$

where $\mathbf{p}^T(\mathbf{x}) = [p_1(\mathbf{x}), p_2(\mathbf{x}), \ldots, p_m(\mathbf{x})]$ is a vector of the complete monomial basis of order m. Examples of $\mathbf{p}^T(\mathbf{x})$ in the 2-D problems are

$$\mathbf{p}^T = (1, x_1, x_2) \text{ for linear basis, } m = 3 \tag{2}$$

$$\mathbf{p}^T = (1, x_1, x_2, x_1^2, x_1x_2, x_2^2) \text{ for quadratic basis, } m = 6 \tag{3}$$

The m unknown parameters $a_j(\mathbf{x})$ can be determined by minimizing the weighted discrete L_2 norm, defined as

$$J(x) = \sum_{i=1}^{n} w(\mathbf{x} - \mathbf{x}_i)[\mathbf{p}^T(\mathbf{x}_i)\mathbf{a}(\mathbf{x}) - \hat{\mathbf{u}}_i]^2 \tag{4}$$

where n is the number of points in the neighborhood of $\boldsymbol{x}$ for which the weight functions $w(\boldsymbol{x} - \boldsymbol{x}_i) > 0$, and $\hat{u}_i$ refers to the nodal parameter of the function u^h at the point $\mathbf{x}_i$. We choose the weight function to have the Gaussian distribution as

$$w(x-x_i)=\begin{cases}\frac{\exp[-(d_i/c_i)^{2k}]-\exp[-(r_i/c_i)^{2k}]}{1-\exp[-(r_i/c_i)^{2k}]} & 0\le d_i\le r_i\\ 0 & d_i\le r_i\end{cases} \quad (5)$$

where $d_i=\|\mathbf{x}-\mathbf{x}_i\|$ is the distance from the sampling point $\boldsymbol{x}$ to the node $\boldsymbol{x}_i$, and r_i is the radius of the domain of influence of the weight function $w(\boldsymbol{x}-\boldsymbol{x}_i)$. Finding the extremum of $J(x)$ in Eq. (4) with respect to $\mathbf{a}(\mathbf{x})$ leads to the following system of linear equation for the determination of $\mathbf{a}(\mathbf{x})$:

$$\mathbf{A}(\mathbf{x})\mathbf{a}(\mathbf{x})=\mathbf{B}(\mathbf{x})\hat{\mathbf{u}} \quad (6)$$

where

$$\mathbf{A}(\mathbf{x})=\sum_{i=1}^{n} w(\mathbf{x}-\mathbf{x}_i)\mathbf{p}(\mathbf{x}_i)\mathbf{p}^T(\mathbf{x}_i) \quad (7)$$

$$\mathbf{B}(\mathbf{x})=[w(\mathbf{x}-\mathbf{x}_1)\mathbf{p}(\mathbf{x}_1), w(\mathbf{x}-\mathbf{x}_2)\mathbf{p}(\mathbf{x}_2),\ldots, w(\mathbf{x}-\mathbf{x}_n)\mathbf{p}(\mathbf{x}_n)] \quad (8)$$

Solving $\mathbf{a}(\mathbf{x})$ from Eq. (6) and substituting it into Eq. (1), the MLS approximation can be defined as

$$u^h(\mathbf{x})=\sum_{i=1}^{n}\phi_i(\mathbf{x})u_i \quad (9)$$

where the shape function is $\phi_i(\mathbf{x})$ defined by

$$\phi_i(\mathbf{x})=\sum_{j=1}^{m} p_j(\mathbf{x})(\mathbf{A}^{-1}(\mathbf{x})\mathbf{B}(\mathbf{x}))_{ji} \quad (10)$$

$\phi_i(\mathbf{x})$ is usually called the shape function of the MLS approximation corresponding to node i. Note that $\phi_i(\mathbf{x}_j)$ does not satisfy the Kronecker delta criterion $\phi_i(\mathbf{x}_j)\neq\delta_{ij}$. Therefore, they are not interpolants, and the name "approximation" is used, that is, $u^h(x_i)\neq\hat{u}_i$ (see Fig. 1 for a simple one-dimensional case for the distinction between u_i and $\hat{u}_i$). For the matrix $\mathbf{A}$ to be invertible, the number of points n must at least equal m ($n\ge m$). In this paper, we choose $m=3$ and $k=1$ in Eq. (9), and take

$$r_i=4c_i \quad (11)$$

where c_i is the distance from node i to its third nearest neighboring node.

B. MLPG Formulation and Discretization

Consider a 2-D elasticity problem in the domain Ω bounded by Γ. The equilibrium equations are

$$\sigma_{ij,j}+b_i=0 \text{ in } \Omega \quad (12)$$

where σ_{ij} is the Cauchy stress tensor and b_i is the body force.

The boundary conditions are as follows:

$$\sigma_{ij}n_j=\bar{t}_i \text{ on } \Gamma_t \quad (13)$$

$$u_j=\bar{u}_i \text{ on } \Gamma_u \quad (14)$$

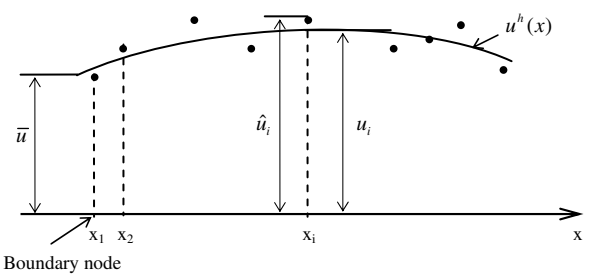

Fig. 1 The distinction between u_i and $\hat{u}_i$.

where $\bar{t}_i$ is defined as the prescribed traction on a surface, $\bar{u}_i$ is the prescribed displacement field, and n_j is the unit outward normal to the boundary Γ. Γ_u and Γ_t are complementary subsets of Γ. A generalized local weak form of Eqs. (12–14) over a local subdomain Ω_s can be written as follows:

$$\int_{\Omega_s}(\sigma_{ij,j}+b_i)v_i\,d\Omega-\int_{\Gamma_u}\alpha(u_i-\bar{u}_i)v_i\,d\Gamma=0 \quad (15)$$

where Γ_u is the part of the boundary of $\partial\Omega_s$ of Ω_s, over which essential boundary conditions are specified. In general $\partial\Omega_s=\Gamma_s\cup L_s$ with Γ_s being the part of the local boundary located on the global boundary and L_s being the other part of the local boundary over which no boundary conditions are specified, that is, $\Gamma_s=\partial\Omega_s\cap\Gamma$ with $\Gamma_s=\partial\Omega_s-L_s$. In Eq. (15), α is a penalty parameter ($\alpha\gg$ Young's modulus/length), which is used to impose the essential boundary conditions. In this paper we choose a value of $\alpha=10^8$. Also, the test functions v_i are chosen such that they vanish on L_s, and this can be accomplished by using the weight function w_i in the MLS approximation as also the test function v_i, but the radius r_i of the support of the weight function is replaced by the radius r_0 of the local domain Ω_s.

Using integration by parts and the divergence theorem in Eq. (15), after some algebraic operations, finally yields the expression in the matrix form as

$$\int_{\Omega_s}\boldsymbol{\varepsilon}_v\boldsymbol{\sigma}\,d\Omega+a\int_{\Gamma_{su}}\mathbf{v}\mathbf{u}\,d\Gamma-\int_{\Gamma_{su}}\mathbf{v}\mathbf{t}\,d\Gamma=\int_{\Gamma_{st}}\mathbf{v}\bar{\mathbf{t}}\,d\Gamma+a\int_{\Gamma_{su}}\mathbf{v}\bar{\mathbf{u}}\,d\Gamma+\int_{\Omega_s}\mathbf{v}\mathbf{b}\,d\Omega \quad (16)$$

In Eq. (16) $\boldsymbol{\sigma}$ is the stress vector derived from the trial functions. That is,

$$\boldsymbol{\sigma}=\begin{Bmatrix}\sigma_{11}\\ \sigma_{22}\\ \sigma_{12}\end{Bmatrix},\qquad \boldsymbol{\varepsilon}_v=\begin{bmatrix}\varepsilon_{11}^{(1)} & \varepsilon_{22}^{(1)} & \gamma_{12}^{(1)}\\ \varepsilon_{11}^{(2)} & \varepsilon_{22}^{(2)} & \gamma_{12}^{(2)}\end{bmatrix} \quad (17)$$

where the superscript j denotes the ith test function. Functions $\mathbf{v}$, $\mathbf{u}$, $\mathbf{t}$, and $\mathbf{b}$ are defined as follows:

$$\mathbf{v}=\begin{bmatrix}v_{11} & v_{12}\\ v_{21} & v_{22}\end{bmatrix},\qquad \mathbf{u}=\begin{Bmatrix}u_1\\ u_2\end{Bmatrix},\qquad \mathbf{t}=\begin{Bmatrix}t_1\\ t_2\end{Bmatrix},\qquad \mathbf{b}=\begin{Bmatrix}b_1\\ b_2\end{Bmatrix} \quad (18)$$

The two sets of test functions $\mathbf{v}$ in Eq. (18) should be linearly independent. The simplest choice for $\mathbf{v}$ as proposed by Atluri [12] is $v_{ij}=v\delta_{ij}$ or $\mathbf{v}=v\mathbf{I}$.

As long as the union of all local subdomains covers the global domain, Eqs. (12–14) will be satisfied in the global domain Ω and on its boundary Γ, respectively. Substituting the MLS approximation Eq. (9) into Eq. (16), and summing over all nodes leads to the following discretized system of linear equations:

$$\sum_{j=1}^{n}\int_{\Omega_s}\boldsymbol{\varepsilon}_v(\mathbf{x},\mathbf{x}_i)\mathbf{D}\mathbf{B}_j\hat{\mathbf{u}}_j\,d\Omega+a\sum_{j=1}^{n}\int_{\Gamma_{su}}\mathbf{v}(\mathbf{x},\mathbf{x}_i)\mathbf{S}\phi_j\hat{\mathbf{u}}_j\,d\Gamma-\sum_{j=1}^{n}\int_{\Gamma_{su}}\mathbf{v}(\mathbf{x},\mathbf{x}_i)\mathbf{N}\mathbf{D}\mathbf{S}\mathbf{B}_j\hat{\mathbf{u}}_j\,d\Gamma=\int_{\Gamma_{st}}\mathbf{v}(\mathbf{x},\mathbf{x}_i)\bar{\mathbf{t}}\,d\Gamma+a\int_{\Gamma_{su}}\mathbf{v}(\mathbf{x},\mathbf{x}_i)\mathbf{S}\bar{\mathbf{u}}\,d\Gamma+\int_{\Omega_s}\mathbf{v}(\mathbf{x},\mathbf{x}_i)\mathbf{b}\,d\Omega \quad (19)$$

where $\mathbf{v}(\mathbf{x},\boldsymbol{x}_i)$ is the value at x of the test function corresponding to node i, and

$$\mathbf{N}=\begin{bmatrix} n_1 & 0 & n_2 \\ 0 & n_2 & n_1 \end{bmatrix} \qquad \mathbf{B}_j=\begin{bmatrix} \phi_{j,1} & 0 \\ 0 & \phi_{j,2} \\ \phi_{j,2} & \phi_{j,1} \end{bmatrix}$$
$$\mathbf{D}=\frac{\bar{E}}{1-\bar{\nu}^2}\begin{bmatrix} 1 & \bar{\nu} & 0 \\ \bar{\nu} & 1 & 0 \\ 0 & 0 & (1-\bar{\nu})/2 \end{bmatrix} \tag{20}$$

$$\bar{E}=\begin{cases} E & \text{for plane stress,} \\ \frac{E}{(1-\nu^2)} & \text{for plane strain,} \end{cases} \qquad \bar{\nu}=\begin{cases} \nu & \text{for plane stress} \\ \frac{\nu}{(1-\nu)} & \text{for plane strain} \end{cases} \tag{21}$$

and

$$S=\begin{bmatrix} S_1 & 0 \\ 0 & S_2 \end{bmatrix}; \qquad S_i=\begin{cases} 1 & \text{if } u_i \text{ is prescribed} \\ 0 & \text{if } u_i \text{ is not prescribed on } \Gamma_u \end{cases} \tag{22}$$

Equation (19) can be simplified into the following system of linear algebraic equations in $\hat{u}_j$:

$$\sum_{j=1}^{N} K_{ij}\hat{u}_j = f_j \qquad i=1,2,\ldots,N \tag{23a}$$

$$\mathbf{K}\,\hat{\mathbf{u}}=\mathbf{f} \tag{23b}$$

where $\hat{\mathbf{u}}$ is the generalized fictitious displacement vector. The so-called stiffness matrix $\mathbf{K}$ and the load vector $\mathbf{f}$ are defined by

$$K_{ij}=\int_{\Omega_s}\boldsymbol{\varepsilon}_v(\mathbf{x},\mathbf{x}_i)\mathbf{D}\mathbf{B}_j\,d\Omega + a\int_{\Gamma_{su}}\mathbf{v}(\mathbf{x},\mathbf{x}_i)\mathbf{S}\boldsymbol{\phi}_j\,d\Gamma - \int_{\Gamma_{su}}\mathbf{v}(\mathbf{x},\mathbf{x}_i)\mathbf{N}\mathbf{D}\mathbf{B}_j\mathbf{S}\,d\Gamma \tag{24}$$

$$f_i=\int_{\Gamma_{st}}\mathbf{v}(\mathbf{x},\mathbf{x}_i)\bar{\mathbf{t}}\,d\Omega + \alpha\int_{\Gamma_{su}}\mathbf{v}(\mathbf{x},\mathbf{x}_i)\mathbf{S}\bar{\mathbf{u}}\,d\Gamma + \int_{\Omega_s}\mathbf{v}(\mathbf{x},\mathbf{x}_i)\mathbf{b}\,d\Gamma \tag{25}$$

As can be seen from Eq. (24) the system "stiffness matrix" is banded but unsymmetric.

C. Generalized Plane Strain Problem

Consider a unidirectional fiber reinforced composite. Introduce the coordinate system as follows. The x_3 axis is aligned with the direction of fibers (assuming fibers are all straight and laid parallel to each other), and the x_1 and x_2 axes all lie in a cross section of the material perpendicular to the fibers. The material is homogeneous in the x_3 direction. When investigating material properties, it is reasonable to assume that composite is subjected to a uniform deformation in the x_3 direction, that is, all the strains are not functions of x_3. The uniformity of the deformation and the material homogeneity in the x_3 direction enables one to simplify the problem of the microscopic deformation of the material from a general three-dimensional problem in the x_1–x_2–x_3 space to a special two-dimensional one in the x_1–x_2 plane, a generalized strain problem as shown by Adams and Crane [2], in which all the strains are functions of x_1 and x_2 only. It implies that the stresses are not functions of x_3 from the constitutive relations for linearly elastic and homogeneous materials. Then the displacements can be written as

$$u=u(x_1,x_2) \qquad v=v(x_1,x_2) \qquad w=w(x_1,x_2)+x_3\varepsilon^0 \tag{26}$$

where ε^0 is the constant macroscopic direct strain in the z direction.

$$\varepsilon^0=\varepsilon_{33} \tag{27}$$

Expressions for the strains can now be simplified according to Eq. (26)

$$\varepsilon_{11}=\frac{\partial u}{\partial x_1}; \qquad \gamma_{12}=\frac{\partial u}{\partial x_2}+\frac{\partial v}{\partial x_1} \qquad \varepsilon_{22}=\frac{\partial v}{\partial x_2}$$
$$\gamma_{13}=\frac{\partial w}{\partial x_1}+\cancel{\frac{\partial \gamma}{\partial x_3}} \qquad \varepsilon_{33}=\frac{\partial w}{\partial x_3}; \qquad \gamma_{23}=\frac{\partial w}{\partial x_2}+\cancel{\frac{\partial \gamma}{\partial x_3}} \tag{28}$$

where $\boldsymbol{\varepsilon}$ represents normal strain and $\boldsymbol{\gamma}$ represents engineering shear strain. The constitutive equations in terms of stress-strain relations are given as

$$\begin{Bmatrix} \sigma_{11} \\ \sigma_{22} \\ \sigma_{33} \\ \sigma_{12} \end{Bmatrix}=\frac{E}{(1+\nu)(1-2\nu)}\begin{bmatrix} 1-\nu & \nu & \nu & 0 \\ \nu & 1-\nu & \nu & 0 \\ \nu & \nu & 1-\nu & 0 \\ 0 & 0 & 0 & \frac{1-2\nu}{2} \end{bmatrix}\begin{Bmatrix} \varepsilon_{11} \\ \varepsilon_{22} \\ \varepsilon_{33} \\ \varepsilon_{12} \end{Bmatrix} \tag{29}$$

The relations can be expressed in a reduced form as

$$\begin{Bmatrix} \sigma_{11} \\ \sigma_{22} \\ \sigma_{12} \end{Bmatrix}=\frac{E}{(1+\nu)(1-2\nu)}\begin{bmatrix} 1-\nu & \nu & 0 \\ \nu & 1-\nu & 0 \\ 0 & 0 & (1-2\nu)/2 \end{bmatrix}\{\varepsilon\} + \begin{bmatrix} \frac{E\nu}{(1+\nu)(1-2\nu)} \\ \frac{E\nu}{(1+\nu)(1-2\nu)} \\ 0 \end{bmatrix}\varepsilon^0 \tag{30}$$

or

$$\{\sigma\}=[D]\{\varepsilon\}+\{F^*\}\varepsilon^0 \tag{31}$$

and

$$\sigma_{33}=\left\{\frac{E\nu}{(1+\nu)(1-2\nu)}\frac{E\nu}{(1+\nu)(1-2\nu)}0\right\}\{\varepsilon\} + \frac{E(1-\nu)}{(1+\nu)(1-2\nu)}\varepsilon^0 \tag{32}$$

or

$$\sigma_{33}=\{F^*\}^T\{\varepsilon\}+\frac{E(1-\nu)}{(1+\nu)(1-2\nu)}\varepsilon^0 \tag{33}$$

where the matrix $\mathbf{D}$ is defined as shown in Eq. (20) for the conventional plane strain problem and

$$\mathbf{F}^*=\begin{bmatrix} \frac{E\nu}{(1+\nu)(1-2\nu)} \\ \frac{E\nu}{(1+\nu)(1-2\nu)} \\ 0 \end{bmatrix} \tag{34}$$

Reactions $\mathbf{t}$ at Γ_u can be expressed as

$$\mathbf{t}=[N][\sigma]=[N][D]\{\varepsilon\}+[N][F^*]\varepsilon^0 \tag{35}$$

where the matrix $\boldsymbol{N}$ is defined in Eq. (20).

Because ε_{33} is constant and prescribed, we can choose the components $\varepsilon_{33}^v=0$ in the strain matrix in Eq. (17) which comes from the test function. Therefore stress σ_{33} will not contribute to Eq. (16), when Eqs. (31) and (35) are substituted into the first and third terms, respectively, of the right-hand side of Eq. (16). After some algebraic operations, finally two terms are added to the load vector in Eq. (25) as shown below, while the stiffness matrix $\mathbf{K}$ in Eq. (24) remains unchanged.

$$f_i=\int_{\Gamma_{st}}\mathbf{v}(\mathbf{x},\mathbf{x}_i)\bar{\mathbf{t}}\,d\Omega + \alpha\int_{\Gamma_{su}}\mathbf{v}(\mathbf{x},\mathbf{x}_i)\mathbf{S}\bar{\mathbf{u}}\,d\Gamma + \int_{\Omega_s}\mathbf{v}(\mathbf{x},\mathbf{x}_i)\mathbf{b}\,d\Gamma - \int_{\Omega_s}\boldsymbol{\varepsilon}_v(\mathbf{x},\mathbf{x_i})\mathbf{F}^*\varepsilon^0\,d\Omega + \int_{\Gamma_{su}}\mathbf{v}(\mathbf{x},\mathbf{x}_i)\mathbf{N}\mathbf{S}\mathbf{F}^*\varepsilon^0\,d\Gamma \tag{36}$$

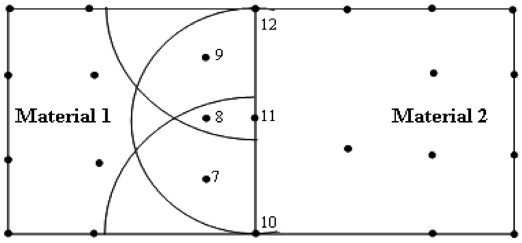

Fig. 2 Illustration of inhomogeneous body.

D. Treatment of Material Discontinuity

In general, the MLS approximation in Eq. (9) does not pass through the nodal data, which are approximate values at nodes. This leads to some difficulties in imposing essential boundary conditions and treating material discontinuity. As mentioned above, a penalty method is used to enforce the essential boundary conditions in this paper. Treatment of material discontinuity is described later.

The current method involves considering the composite as two separate homogeneous bodies and then applying interface conditions to reconnect the bodies. For example, let us consider a two-phase problem as shown in Fig. 2. The composite is separated into two homogeneous parts. In each part, we have the weak form of the problem as described above; the continuity of tractions at interface is weakly satisfied at the variational level. We will determine the actual displacements at the interface, and after that, conditions of continuity of displacements at the interface can also be directly enforced as in the FE method.

In this method common nodes are used at the interface that belongs to both materials. In Fig. 2 nodes (10–12) are defined at the interface of materials 1 and 2. We use the following example to illustrate the proposed method.

For material 1: Assume that neighbors of point 10 include 7, 8, 10, and 11; neighbors of point 11 include 7, 8, 9, 10, 11, and 12; neighbors of 12 include 8, 9, 11, and 12.

Consider the following MLS approximation:

$$\tilde{u}(x) = \sum_{i=1}^{n} \phi_i(x)\hat{u}_i \tag{37}$$

such that at points x_j we have the actual displacements as

$$\tilde{u}_j = \sum_{i=1}^{n} \phi_i(x_j)\hat{u}_i \tag{38}$$

For nodes at the interface, we have

$$\begin{aligned}
\tilde{u}_{10} &= \phi_7(x_{10})\hat{u}_7 + \phi_8(x_{10})\hat{u}_8 + \phi_{10}(x_{10})\hat{u}_{10} + \phi_{11}(x_{10})\hat{u}_{11} \\
\tilde{u}_{11} &= \phi_7(x_{11})\hat{u}_7 + \phi_8(x_{11})\hat{u}_8 + \phi_{10}(x_{11})\hat{u}_{10} + \phi_{11}(x_{11})\hat{u}_{11} \\
&\quad + \phi_{12}(x_{11})\hat{u}_{12} \\
\tilde{u}_{12} &= \phi_8(x_{12})\hat{u}_8 + \phi_9(x_{12})\hat{u}_g + \phi_{11}(x_{12})\hat{u}_{11} + \phi_{12}(x_{12})\hat{u}_{12}
\end{aligned} \tag{39}$$

In matrix form:

$$\begin{Bmatrix} \tilde{u}_{10} \\ \tilde{u}_{11} \\ \tilde{u}_{12} \end{Bmatrix} = \begin{bmatrix} \phi_7(x_{10}) & \phi_8(x_{10}) & 0 & \phi_{10}(x_{10}) & \phi_{11}(x_{10}) & 0 \\ \phi_7(x_{11}) & \phi_8(x_{11}) & \phi_9(x_{11}) & \phi_{10}(x_{11}) & \phi_{11}(x_{11}) & \phi_{12}(x_{11}) \\ 0 & \phi_8(x_{12}) & \phi_9(x_{12}) & 0 & \phi_{11}(x_{12}) & \phi_{12}(x_{12}) \end{bmatrix} \times \begin{Bmatrix} \hat{u}_7 \\ \hat{u}_8 \\ \hat{u}_9 \\ \hat{u}_{10} \\ \hat{u}_{11} \\ \hat{u}_{12} \end{Bmatrix} \tag{40}$$

The variables can be partitioned into two subsets as follows:

$$\{\tilde{u}_b\} = \begin{bmatrix} [\phi_r] & [\phi_b] \end{bmatrix} \begin{Bmatrix} \{\hat{u}_r\} \\ \{\hat{u}_b\} \end{Bmatrix} = [\boldsymbol{\varphi}_b]\{\hat{u}\} \tag{41}$$

where $b = 10$, 11, and 12 denotes the nodes on the interface, and $r = 7$, 8, and 9 denotes the nodes which do not lie on the interface.

Expanding the matrix $[\boldsymbol{\varphi}_b]$ to explicitly show the x and y directions, we have

$$\boldsymbol{\varphi}_b = \begin{bmatrix} \cdots & \cdots & \cdots & \cdots & \cdots & \cdots & \cdots \\ \phi_1(x_{bi}) & 0 & \phi_2(x_{bi}) & 0 & \cdots & \phi_N(x_{bi}) & 0 \\ 0 & \phi_1(x_{bi}) & 0 & \phi_2(x_{bi}) & \cdots & 0 & \phi_N(x_{bi}) \\ \cdots & \cdots & \cdots & \cdots & \cdots & \cdots & \cdots \end{bmatrix} \tag{42}$$

where x_{bi}, $b_i = b_1, b_2, \ldots, bn_b$ are the coordinates of nodes at interface.

$[\boldsymbol{\varphi}_b]$ is a $2n_b \times 2N$ matrix, $[\phi_r]$ is a $2n_b \times 2n_r$ matrix, and $[\phi_b]$ is a $2n_b \times 2n_b$ matrix; $[\hat{u}_r]$ is a $2n_r \times 1$ vector, and $[\hat{u}_b]$ is a $2n_b \times 1$ vector; all are known matrices.

Furthermore n_b is the number of nodes on interface, n_r is the number of nodes which do not lie on the interface, and $n_b + n_r = N$ is the total number of nodes in body.

According to Eq. (41), we can compute the fictitious displacements at interface as

$$\{\hat{u}_b\} = [\phi_b]^{-1}[-[\phi_r]\{\hat{u}_r\} + \{\hat{u}_b\}] \tag{43}$$

We can rewrite (23b) as

$$\begin{bmatrix} [K_r] & [K_b] \end{bmatrix} \begin{Bmatrix} \{\hat{u}_r\} \\ \{\hat{u}_b\} \end{Bmatrix} = \{f\} \tag{44}$$

where $[K_b]$ is a known $2N \times 2n_b$ matrix, and $[K_r]$ is a known matrix of size $2N \times 2n_r$.

Substituting Eq. (43) into Eq. (44) and after some algebraic operations we obtain

$$[K]\{u\} = \{f\} \tag{45}$$

$$[K] = \begin{bmatrix} [[K_r] - [K_b][\phi_b]^{-1}[\phi_r] & [[K_b][\phi_b]^{-1}] \end{bmatrix} \qquad \{u\} = \begin{Bmatrix} \{\hat{u}_r\} \\ \{\hat{u}_b\} \end{Bmatrix} \tag{46}$$

$\tilde{u}_b$ is the actual displacement vector at interface.

We use the same procedure for material 2. Therefore, the method presented here is the same as in the FE method. It means that we can use common nodes at the interface, and the conditions of continuity of the interface displacements can also be directly enforced. Note that $[\boldsymbol{\varphi}_b]$ is a very sparse matrix, and one should choose as many points as possible on the interface.

In fact, we can use this technique to enforce the essential boundary conditions, instead of using the penalty method. However we use the technique only to treat the material discontinuity and not for essential boundary conditions to avoid the computational burden of dealing with large size matrices and also to avoid reshaping the global stiffness matrix many times.

III. MLPG-Based Micromechanical Model for Fiber Composites

We demonstrate the MLPG-based micromechanical model to predict the effective stiffness properties for a fiber composite.

The micromechanical analysis of the unidirectional fiber composite is performed by analyzing the unit cell of the composite using the MLPG method. We assume that uniform macrostresses exist through the composite. It is assumed that the fibers are circular in cross section packed in a square array. Thus the unit cell or the representative volume element is a square. The unit cell is shown in

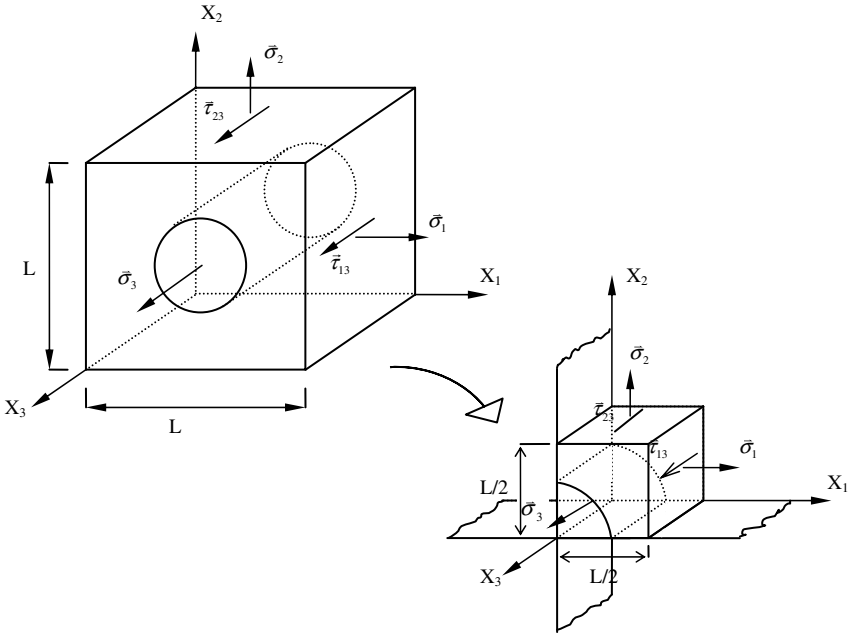

Fig. 3 Unit cell coordinate system.

Fig. 3. The unit cell analysis assumes that the composite is under a uniform state of strain at the macroscopic scale. However the actual stresses in the fiber and the matrix within the unit cell will have spatial variation. These stresses are called microstresses. The macrostresses are average stresses required to create a given state of macrodeformations, and they can be computed from the microstresses obtained from the MLPG method as

$$\sigma_{ij}^{M} = \frac{1}{V}\int_{A} \sigma_{ij}\, \mathrm{d}V \tag{47}$$

where V is volume of the unit cell. The macrostresses and macrostrains are related by the elastic constants of the homogeneous composite $[C]$:

$$\begin{Bmatrix} \sigma_{11}^{M} \\ \sigma_{22}^{M} \\ \sigma_{33}^{M} \\ \tau_{23}^{M} \\ \tau_{31}^{M} \\ \tau_{12}^{M} \end{Bmatrix} = \begin{bmatrix} c_{11} & c_{12} & c_{13} & c_{14} & c_{15} & c_{16} \\ & c_{22} & c_{23} & c_{24} & c_{25} & c_{26} \\ & & c_{33} & c_{34} & c_{35} & c_{36} \\ & & & c_{44} & c_{45} & c_{46} \\ & \text{Symm.} & & & c_{55} & c_{56} \\ & & & & & c_{66} \end{bmatrix} \begin{Bmatrix} \varepsilon_{11}^{M} \\ \varepsilon_{22}^{M} \\ \varepsilon_{33}^{M} \\ \gamma_{23}^{M} \\ \gamma_{31}^{M} \\ \gamma_{12}^{M} \end{Bmatrix} \quad \text{or}$$

$$\{\sigma^{M}\} = [C]\{\varepsilon^{M}\} \tag{48}$$

In the micromechanical analysis, the unit cell is subjected to six linearly independent macroscopic deformations. In each deformation case one of the six macrostrains is assumed to be nonzero and the rest of the macrostrains are set equal to zero. The six cases are as follows: case 1: $\varepsilon_{11}^{M} = 1$; case 2: $\varepsilon_{22}^{M} = 1$; case 3: $\varepsilon_{33}^{M} = 1$; case 4: $\gamma_{12}^{M} = 1$; case 5: $\gamma_{23}^{M} = 1$; case 6: $\gamma_{31}^{M} = 1$. The periodic boundary conditions for these six cases are shown in Table 1. Details of deriving the periodic boundary conditions can be found in [3].

In this paper, we use the micromechanical model to predict the stiffness properties of composites for cases 1–3 only. For case 3, $\varepsilon_{33}^{M} = 1$, the problem is solved as a generalized plane strain problem.

IV. Results and Discussions

In this section, we give two examples along with some discussions for the current method. The first example is a two-phase problem in the plane stress state for investigating the material discontinuity; the second is the analysis of the unit cell for predicting the stiffness properties of a fiber composite containing the cases of the generalized/or conventional plane strain, and the material discontinuity at interface is also investigated.

A. Two-Phase Verification Problem

The MLPG method results are compared to the FEM numerical solution (ABAQUS^{TM}) for the two-phase problem (see Fig. 4). The material properties used for this study are $E_f = 70$, $\nu_f = 0.2$; $E_m = 3.5$, $\nu_m = 0.35$ and the fiber volume fraction $V_f = 0.503$; the boundary is represented as a unit square $a = 1$ and the radius of fiber $R = 0.8$. The MLPG scheme with 183 nodes is used and the uniform load $P = 1$ is applied at its right side as shown in Fig. 4. A state of plane stress normal to the x_1–x_2 plane is assumed.

Figures 5–7 show the comparison of radial and horizontal displacements between the current method and the FE method at the fiber-matrix interface, and along lines $y = 0$ and $x = 1$. We realize

Table 1 Periodic boundary conditions for the MLPG method

Case	Constraints between left and right faces	Constraints between top and bottom faces	Out-of-plane strains
$\varepsilon_{11} = 1$	$u_1(L, x_2) - u_1(0, x_2) = L$ $u_2(L, x_2) - u_2(0, x_2) = 0$	$u_i(x_1, L) - u_i(x_1, 0) = 0$ $i = 1, 2$	$\varepsilon_{33} = 0, \gamma_{31} = 0, \gamma_{23} = 0$
$\varepsilon_{22} = 1$	$u_i(L, x_2) - u_i(0, x_2) = 0$ $i = 1, 2$	$u_1(x_1, L) - u_1(x_1, 0) = 0$ $u_2(x_1, L) - u_2(x_1, 0) = L$	$\varepsilon_{33} = 0, \gamma_{31} = 0, \gamma_{23} = 0$
$\varepsilon_{33} = 1$	$u_i(L, x_2) - u_i(0, x_2) = 0$ $i = 1, 2$	$u_i(x_1, L) - u_i(x_1, 0) = 0$ $i = 1, 2$	$\varepsilon_{33} = 0, \gamma_{31} = 0, \gamma_{23} = 0$
$\gamma_{12} = 1$	$u_1(L, x_2) - u_1(0, x_2) = 0$ $u_2(L, x_2) - u_2(0, x_2) = L$	$u_i(x_1, L) - u_i(x_1, 0) = 0$ $i = 1, 2$	$\varepsilon_{33} = 0, \gamma_{31} = 0, \gamma_{23} = 0$
$\gamma_{23} = 1$	$u_3(L, x_2) - u_3(0, x_2) = 0$	$u_3(x_1, L) - u_3(x_1, 0) = L$	$\varepsilon_{33} = 0, \gamma_{31} = 0$
$\gamma_{31} = 1$	$u_3(L, x_2) - u_3(0, x_2) = L$	$u_3(x_1, L) - u_3(x_1, 0) = 0$	$\varepsilon_{33} = 0, \gamma_{23} = 0$

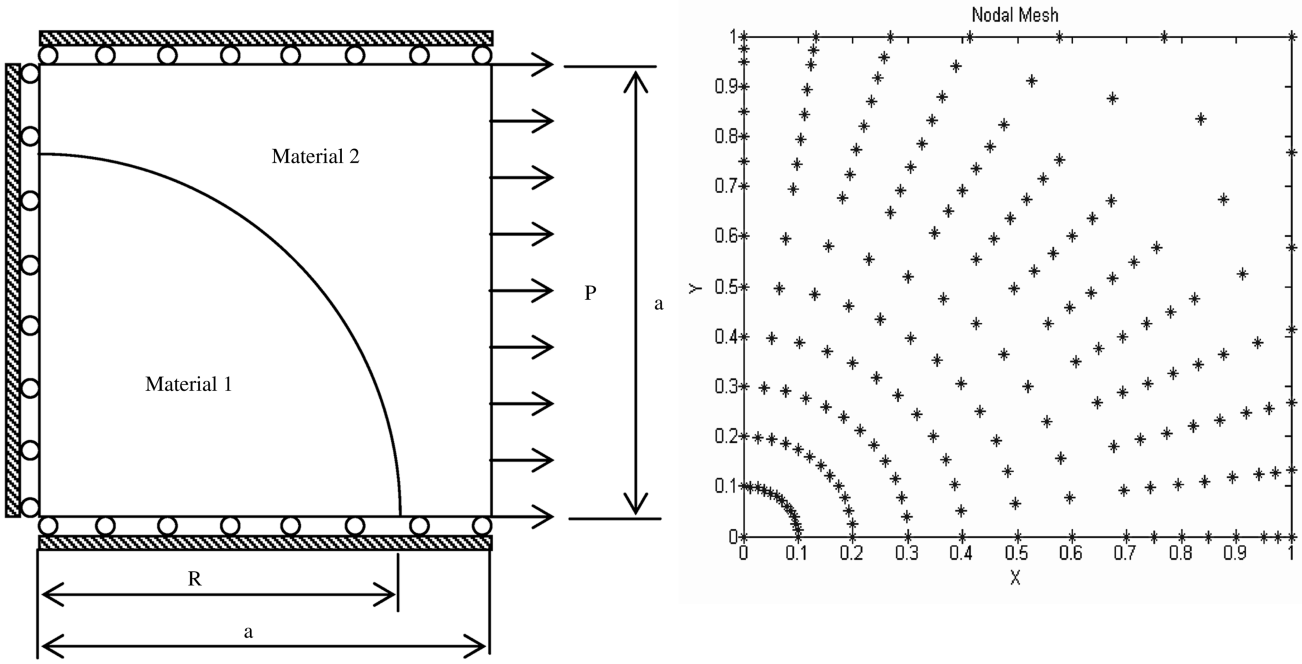

Fig. 4 Depiction of the two-phase problem and corresponding nodes (183 nodes) for the MLPG method.

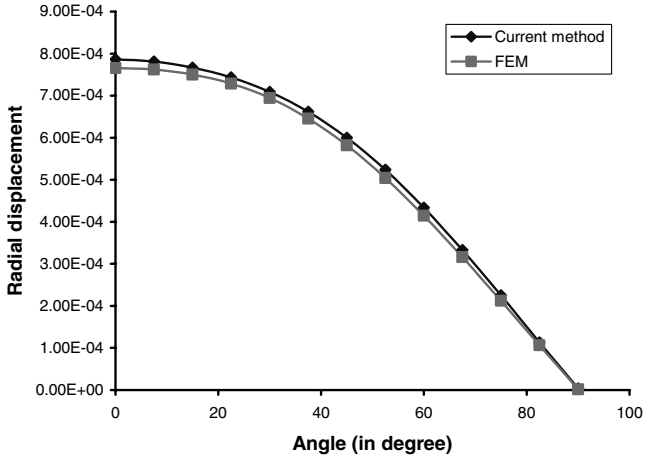

Fig. 5 Comparison of radial displacements at the interface.

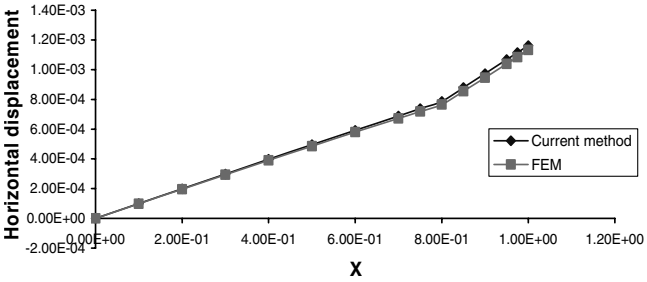

Fig. 6 Comparison of horizontal displacements along line $y = 0$.

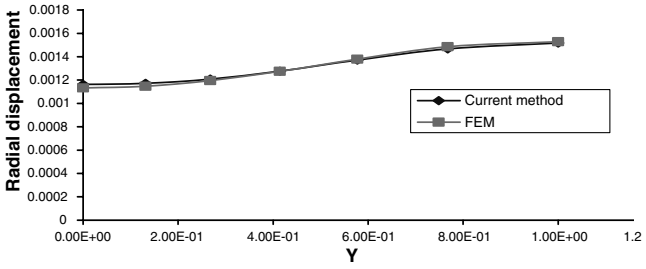

Fig. 7 Comparison of radial displacements along line $x = 1$.

that the current method's solutions are very close to those of the FEM, which are computed using the ABAQUS™ software.

Figures 8–10 show the distribution of interfacial stresses at interface; we can see that the radial and the tangential stresses in the two materials are identical at the interface. The hoop stress in the two materials along the interface is not identical as expected.

The comparison of interfacial stresses with that from the FEM is shown in Figs. 11 and 12. They show that the radial stresses and the

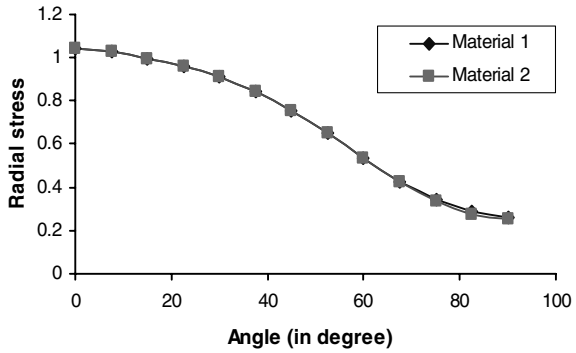

Fig. 8 Radial stresses in the two materials at the interface by MLPG-based micromechanics (current method).

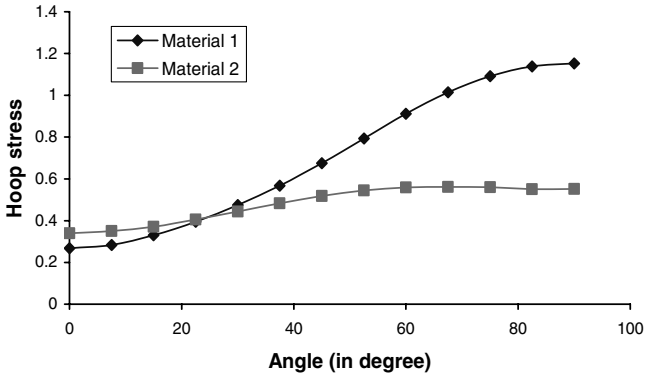

Fig. 9 Hoop stresses in the two materials at the interface by MLPG-based micromechanics.

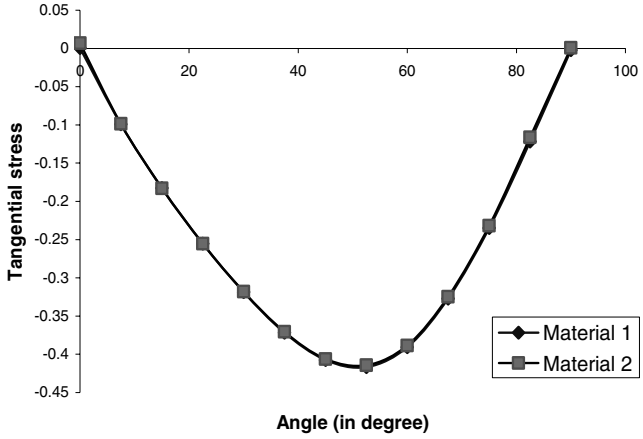

Fig. 10 Tangential (shear) stresses in the two materials at the interface by MLPG-based micromechanics.

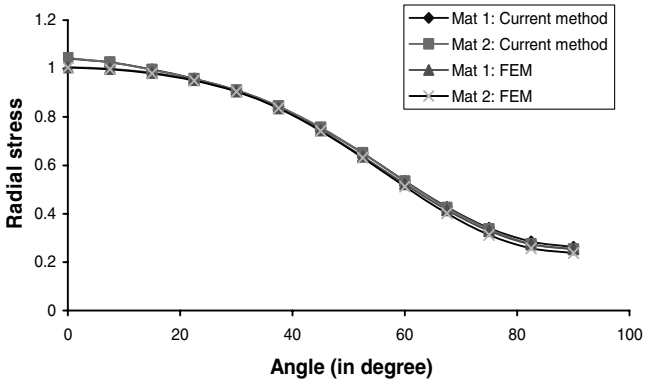

Fig. 11 Comparison of radial stresses at the interface.

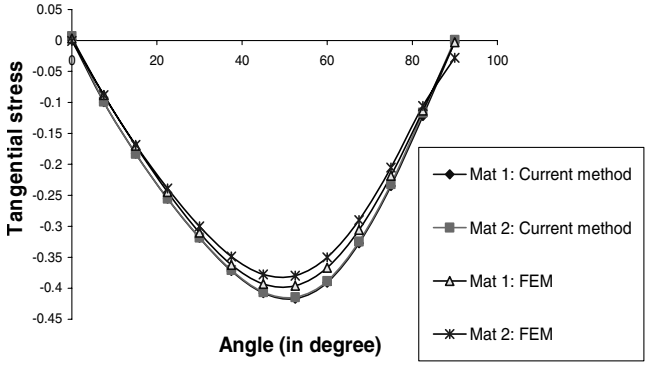

Fig. 12 Comparison of tangential stresses at the interface.

tangential stress for the two materials obtained by the MLPG micromechanics are in good agreement with the FEM results and achieve a significantly higher degree of agreement of the radial and the tangential stresses in the two materials at the interface with a smaller number of degrees of freedom compared to the FEM. The accuracy of stress computation obtained from the current method may be a good aspect in modeling the damage, especially progressive damage, which requires an accurate description of the stress field in different phases.

B. Micromechanics of Unidirectional Fiber Composite

The unidirectional fiber composite was assumed to have circular fibers packed in a square array. The fiber and matrix materials were assumed isotropic, and their properties for this study are $E_f = 70$ GPa, $\nu_f = 0.2$; $E_f = 3.5$ GPa, $\nu_m = 0.35$. Because of symmetry, only one-quarter of the unit cell is modeled, and the fiber volume fraction $V_f = 0.503$; the boundary is represented as a square with a side dimension of 1 ($a = 1$), and the radius of fiber $R = 0.8$. The MLPG method with 183 nodes is used. The displacements applied on the boundaries corresponding to cases 1, 2, and 3 are shown in Table 1. The composite is assumed to be in a state of plane strain normal to the x_1–x_2 plane. Figure 13 represents the tension tests in the x_1 and x_2 directions ($\varepsilon_{22}^M = 1$ and $\varepsilon_{22}^M = 1$) by imposing a specified uniform displacement $\bar{u} = 1$ on the unit cell.

The microstresses are computed by the MLPG method, and then the average stresses are computed using Eq. (47), and finally the stiffness properties C_{ij} can be also computed by Eq. (48). From the stiffness coefficients C elastic constants are computed and they are presented in Table 2. The subscripts of the elastic constants have been changed to conform to the convention use in the literature of composite mechanics in Table 2.

The elastic constants computed using the current method are very close to those obtained by the Halpin–Tsai equations [27]. The maximum error is 2.45% for E_2 and E_3, 1.16% for ν_{21} and ν_{31}, and 1.82% for ν_{12} and ν_{13}. The minimum error obtained is 0.14% for E_1. Note that the Halpin–Tsai formulas are not available for ν_{23} and ν_{32}.

Figure 14 shows the distribution of interfacial stresses for the case $\varepsilon_{11} = 1$, and Fig. 15 shows the distribution of interfacial stresses for the case $\varepsilon_{33} = 1$. Both the figures show that the radial and tangential stresses are continuous at the material interface, but there is a jump at the interface for hoop stresses as expected. Note that the x_1, x_2, and x_3 directions shown in these figures are the same as in Fig. 3. Because of symmetry (see Fig. 13), the distribution of stresses for the case $\varepsilon_{22} = 1$ is the same as the case $\varepsilon_{11} = 1$.

V. Conclusions

From the above results and discussions we can reach the following conclusions:

1) The technique of direct imposition of interface boundary conditions is used for the first time for the treatment of the material discontinuity at the interface in the MLPG method. The current

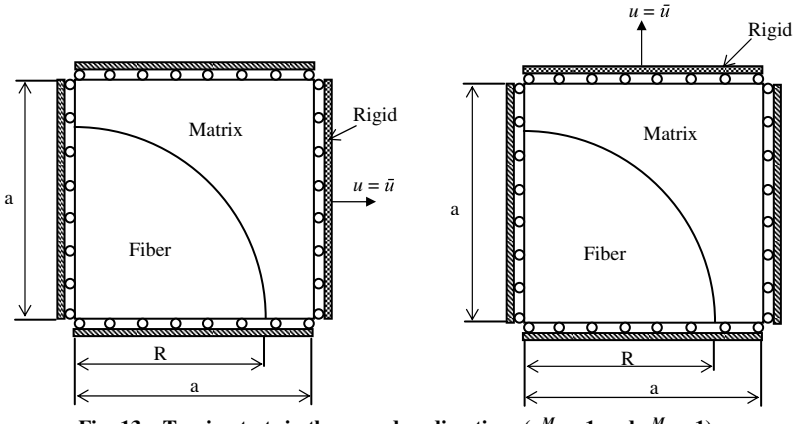

Fig. 13 Tension tests in the x_1 and x_2 directions ($\varepsilon_{11}^M = 1$ and $\varepsilon_{22}^M = 1$).

Table 2 Comparison of elastic constants between the current method and Halpin–Tsai equations. Moduli are in GPa

Method	E_1	E_2	E_3	ν_{12}	ν_{21}	ν_{13}	ν_{31}	ν_{23}	ν_{32}
Current method	36.90	11.848	11.848	0.280	0.085	0.280	0.085	0.315	0.315
Halpin–Tsai	36.95	11.565	11.565	0.275	0.086	0.275	0.086	——	——

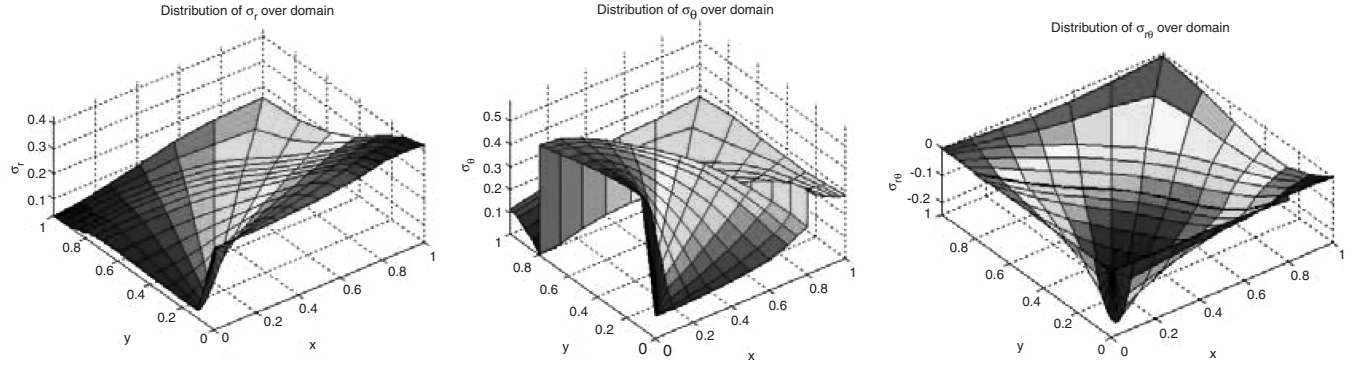

Fig. 14 Distribution of interfacial stresses for the case $\varepsilon_{11} = 1$ (σ_r is scaled by 1/50, $\sigma_{r\theta}$ and σ_θ are scaled by 1/30).

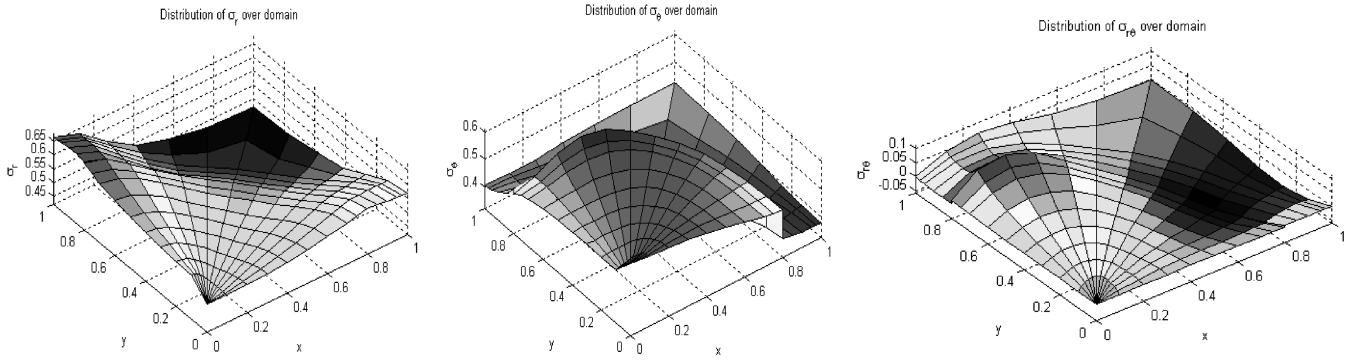

Fig. 15 Distribution of interfacial stresses for the case $\varepsilon_{33} = 1$ (σ_r is scaled by 1/7, $\sigma_{r\theta}$ and σ_θ are scaled by 1/10).

method shows good agreement with the FEM solution and achieves a significantly higher degree of agreement between the radial and tangential stresses in the two materials at the interface with a smaller number of degrees of freedom compared to the FEM.

2) The MLPG method is additionally formulated for the generalized plane strain problems. The elastic constants obtained by the MLPG-based micromechanical model match very well with available results.

3) The current method is a truly meshless method, wherein no elements or background cells are involved, either in the interpolation or in the integration.

The current method shows promise in the application to the micromechanics of textile composites where the complexities and inaccuracies involved in the FE mesh can be avoided.

Acknowledgements

The authors are grateful to the Vietnam Education Foundation for the fellowship granted to Thi Dang. Partial support was provided by the Army Research Office Contract DAAD19-02-1-0330 with Bruce LaMattina as the Grant Monitor.

References

[1] Adams, D. F., and Doner, D. R., "Longitudinal Shear Loading of a Unidirectional Composites," *Journal of Composite Materials*, Vol. 1, 1967, pp. 4–17.

[2] Adams, D. F., and Crane, D. A., "Finite Element Micromechanical Analysis of a Unidirectional Composite Including Longitudinal Shear Loading," *Computers and Structures*, Vol. 18, No. 6, 1984, pp. 1153–1165.

[3] Marrey, R. V., and Sankar, B. V., "Micromechanical Models for Textile Structural Composites," NASA CR-198229, Oct. 1995.

[4] Pipes, R. B., and Pagano, N. J., "Interlaminar Stresses in Composite Laminates Under Uniform Axial Extension," *Journal of Composite Materials*, Vol. 4, 1970, pp. 538–548.

[5] Pagano, N. J., and Soni, S. R., "Global-Local Laminate Variational Model," *International Journal of Solids and Structures*, Vol. 19, No. 3, 1983, pp. 207–228.

[6] Li, S., and Lim, S. H., "Variational Principles for Generalised Plane Strain Problems and Their Applications," *Composites Part A*, Vol. 36, No. 3, 2005, pp. 353–365.

[7] Kim, H. J., and Swan, C. C., "Voxel-Based Meshing and Unit-Cell Analysis of Textile Composites," *International Journal for Numerical Methods in Engineering*, Vol. 56, No. 7, 2003, pp. 977–1006.

[8] Marrey, R. V., and Sankar, B. V., "A Micromechanical Model for Textile Composite Plates," *Journal of Composite Materials*, Vol. 31, No. 12, 1997, pp. 1187–1213.

[9] Zhu, H., Sankar, B. V., and Marrey, R. V., "Evaluation of Failure Criteria for Fiber Composites Using Finite Element Micromechanics," *Journal of Composite Materials*, Vol. 32, No. 8, 1998, pp. 766–782.

[10] Sankar, B. V., and Marrey, R. V., "Analytical Method for Micromechanics of Textile Composites," *Composites Science and Technology*, Vol. 57, No. 6, 1997, pp. 703–713.

[11] Karkkainen, R. L., and Sankar, B. V., "A Direct Micromechanics Method for Analysis of Failure Initiation of Plain Weave Textile Composites," *Composites Science and Technology*, Vol. 66, No. 1, 2006, pp. 137–150.

[12] Atluri, S. N., and Zhu, T. L., "The Meshless Local Petrov-Galerkin (MLPG) Approach For Solving Problems In Elasto-Statics," *Computational Mechanics*, Vol. 25, Nos. 2–3, 2000, pp. 169–179.

[13] Atluri, S. N., Kim, H. G., and Cho, J. Y., "A Critical Assessment of the Truly Meshless Local Petrov-Galerkin (MLPG), and Local Boundary Integral Equation (LBIE) Methods," *Computational Mechanics*,

Vol. 24, No. 5, 1999, pp. 349–372.
[14] Raju, I. S., and Chen, T., "Meshless Petrov-Galerkin Method Applied to Axisymmetric Problems," *AIAA/ASME/ASCE/AHS/ASC Structures, Structural Dynamics, and Materials Conference and Exhibit, 42nd*, AIAA, Reston, VA, 16–19 April 2001.
[15] Raju, I. S., and Phillips, D. R., "Local Coordinate Approach in Meshless Local Petrov-Galerkin Method for Beam Problems," *AIAA Journal*, Vol. 41, No. 5, 2003, pp. 975–978.
[16] Ching, H. K., and Batra, R. C., "Determination of Crack Tip Fields in Linear Elastostatics by the Meshless Local Petrov-Galerkin (MLPG) Method," *Computer Modeling in Engineering and Sciences*, Vol. 2, No. 2, 2001, pp. 273–289.
[17] Batra, R. C., and Ching, H. K., "Analysis of Elastodynamic Deformations Near a Crack/Notch Tip by the Meshless Local Petrov-Galerkin (MLPG) Method," *Computer Modeling in Engineering and Sciences*, Vol. 3, No. 6, 2002, pp. 717–730.
[18] Cordes, L. W., and Moran, B., "Treatment of Material Discontinuity in the Element-Free Galerkin Method," *Computer Methods in Applied Mechanics and Engineering*, Vol. 139, Nos. 1–4, 1996, pp. 75–89.
[19] Krongauz, Y., and Belytschko, T., "EFG Approximation with Discontinuous Derivatives," *International Journal for Numerical Methods in Engineering*, Vol. 41, No. 7, 1998, pp. 1215–1233.
[20] Cai, Y. C., and Zhu, H. H., "Direct Imposition of Essential Boundary Conditions and Treatment of Material Discontinuities in the EFG Method," *Computational Mechanics*, Vol. 34, No. 4, 2004, pp. 330–338.
[21] Batra, R. C., Porfiri, M., and Spinello, D., "Treatment of Material Discontinuity in Two Meshless Local Petrov-Galerkin (MLPG) Formulations of Axisymmetric Transient Heat Conduction," *International Journal for Numerical Methods in Engineering*, Vol. 61, No. 14, 2004, pp. 2461–2479.
[22] Dang, T. D., and Sankar, B. V., "Meshless Local Petrov-Galerkin Micromechanical Analysis of Fiber Composites Including Axial Shear Loading," *7th World Congress on Computational Mechanics*, OminPress, Madison, WI, 16–22 July 2006.
[23] Belytschko, T., Krongauz, Y., Organ, D., Fleming, M., and Krysl, P., "Meshless Methods: An Overview and Recent Developments," *Computer Methods in Applied Mechanics and Engineering*, Vol. 139, Nos. 1–4, 1996, pp. 3–47.
[24] Atluri, S. N., *The Meshless Method (MLPG) for Domain & BIE Discretizations*, Tech Science Press, Forsyth, GA, 2004.
[25] Atluri, S. N., and Shen, S., "The Meshless Local Petrov-Galerkin (MLPG) Method: A Simple and Less-Costly Alternative to the Finite Element and Boundary Element Methods," *Computer Modeling in Engineering and Sciences*, Vol. 3, No. 1, 2002, pp. 11–52.
[26] Lancaster, P., and Salkauskas, K., "Surface Generated by Moving Least Squares Methods," *Mathematics of Computation*, Vol. 37, No. 155, 1981, pp. 141–158.
[27] Gibson, R. F., *Principles of Composite Material Mechanics*, McGraw–Hill, New York, 1994.

A. Roy
Associate Editor